Supplement of Solid Earth, 15, 747–762, 2024
https://doi.org/10.5194/se-15-747-2024-supplement

Solid Earth Open Access EGU

Supplement of

Propagating rifts: the roles of crustal damage and ascending mantle fluids

Folarin Kolawole and Rasheed Ajala

Correspondence to: Folarin Kolawole (fola@ldeo.columbia.edu)

Supplement

Contents of this file

Figures S1 to S24

Introduction

This supplementary document contains supplemental figures (Figures S1 – S24) supporting the results and conclusions in the main manuscript.

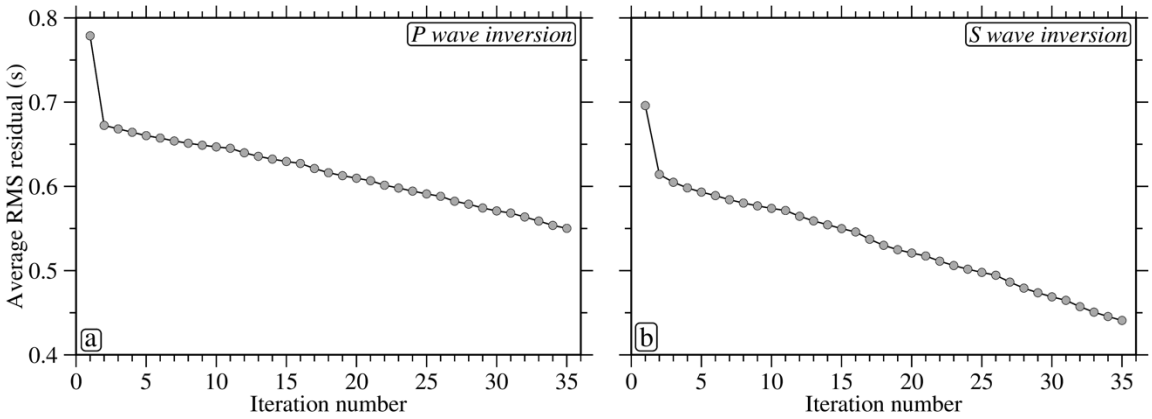

Figure S1. Average RMS travel time residuals for the (**a**) P and (**b**) S inversion.

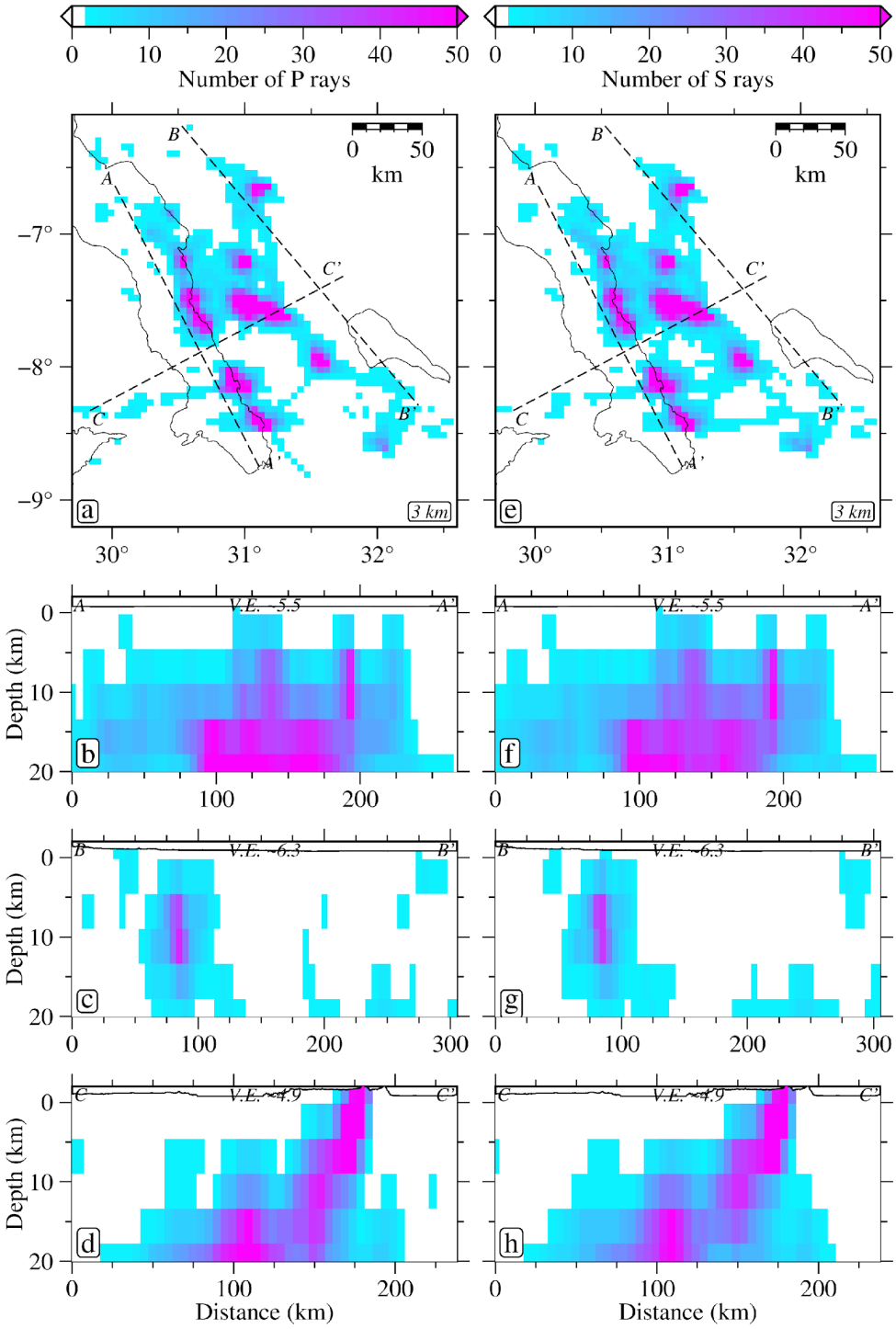

Figure S2. Ray coverage maps for the inversion. (**a** – **d**). Maps and profiles for the P wave model. (**e** –**h**) Maps and profiles for the S wave model.

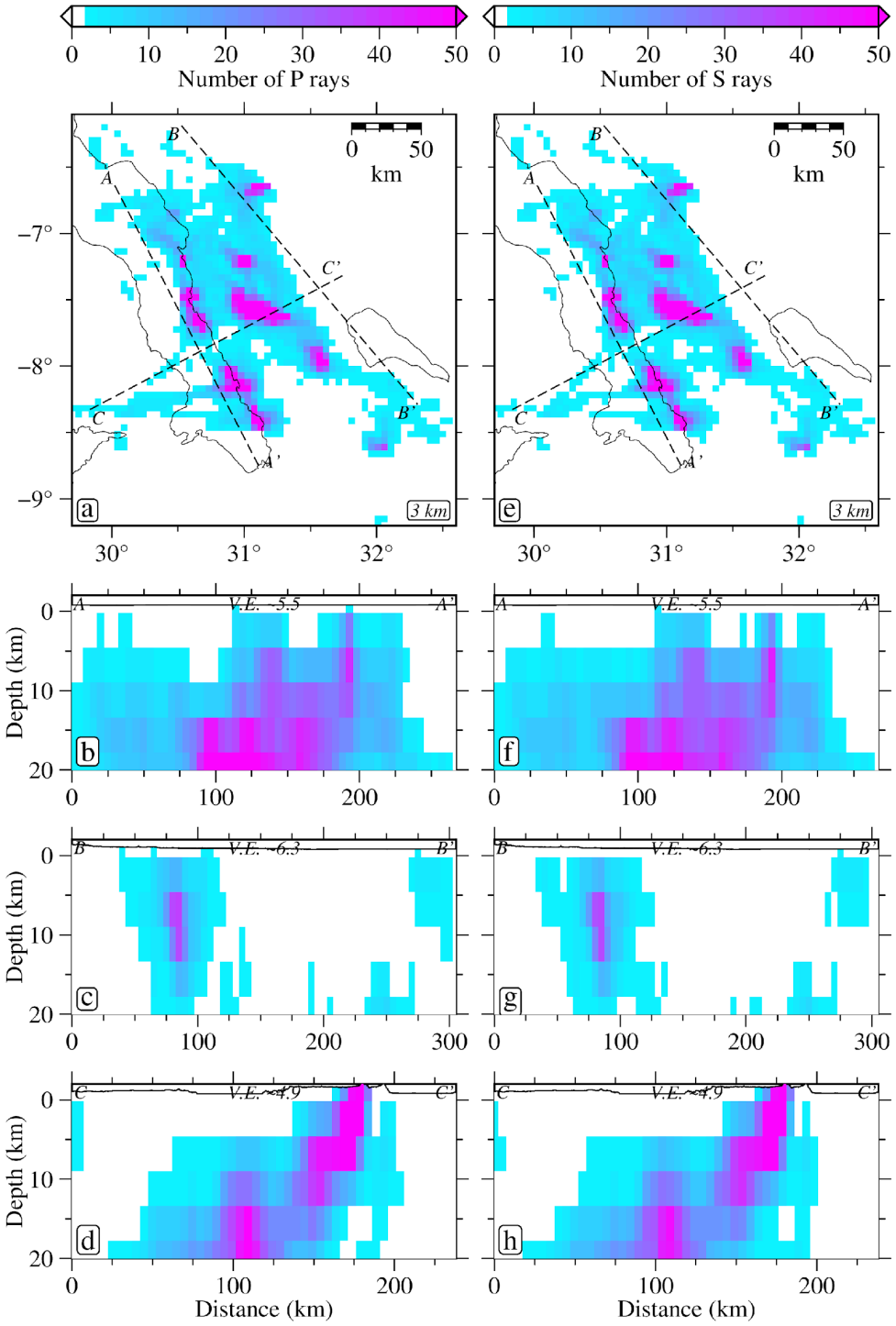

Figure S3. Same as Fig. S2 but for the synthetic model inversion.

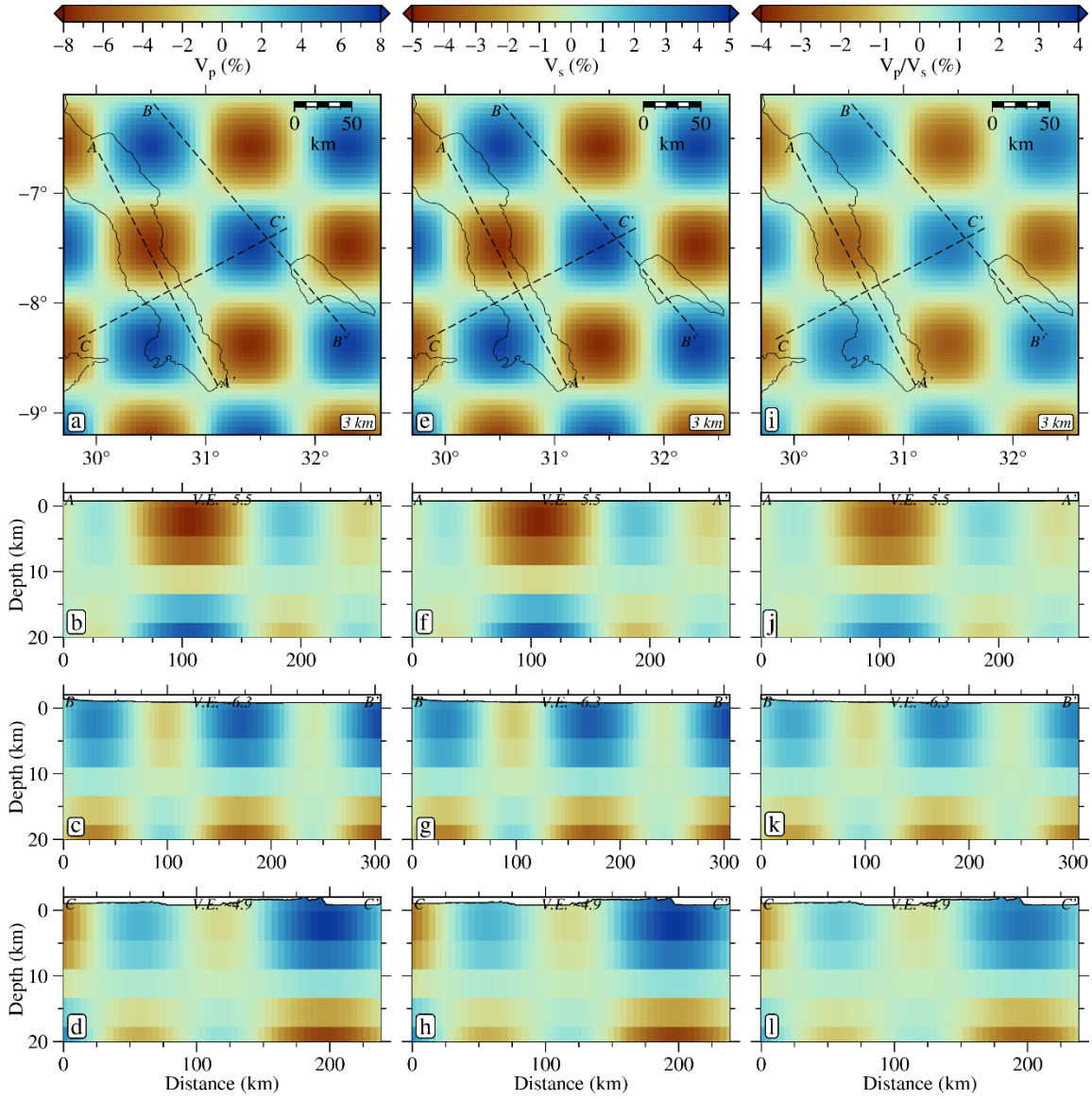

Figure S4. True synthetic model with 100 km x 100 km x 25 km checkers.

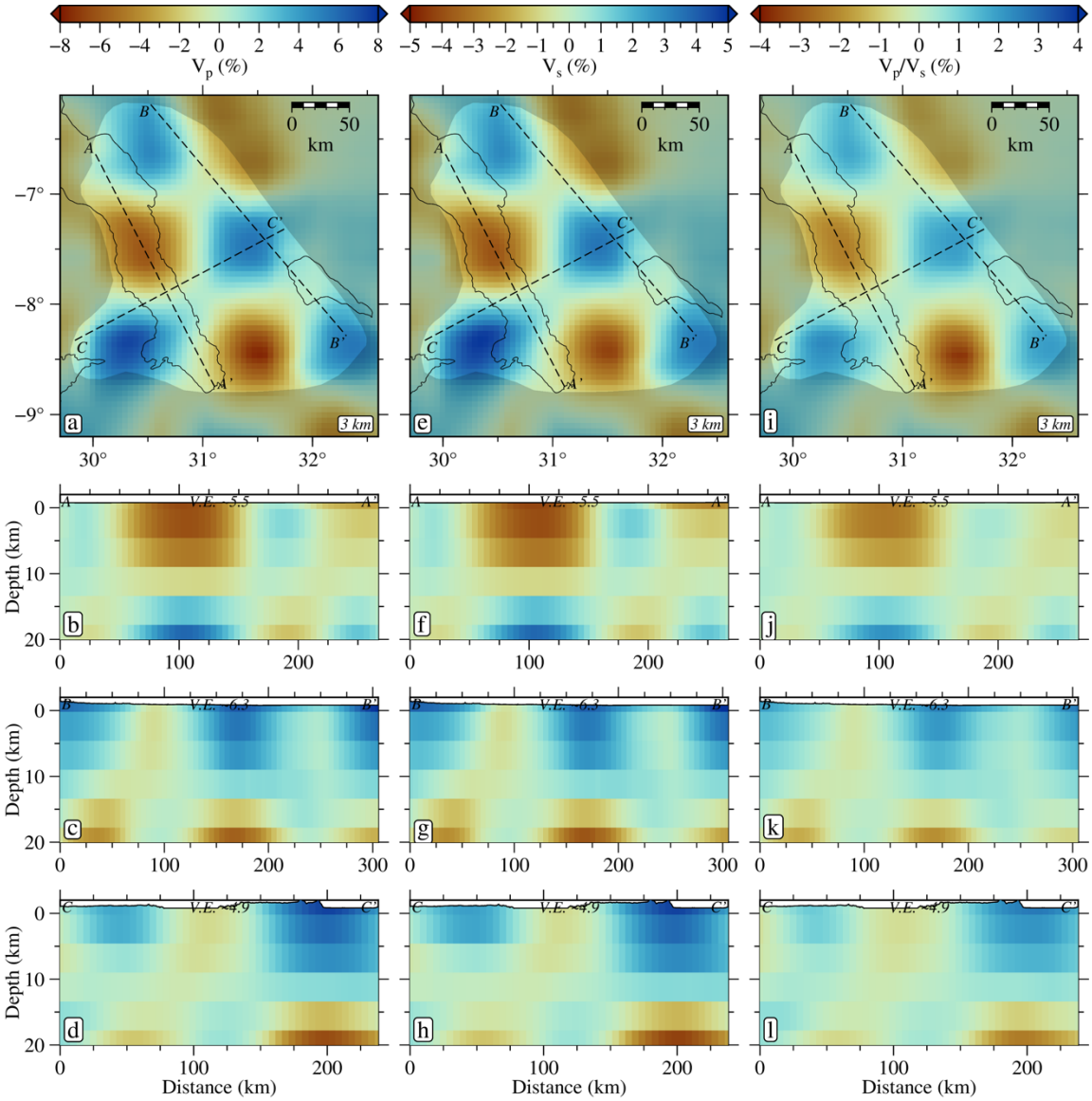

Figure S5. Recovered synthetic model with 100 km x 100 km x 25 km checkers. Unreliable areas of the models are lightly grayed out on the maps.

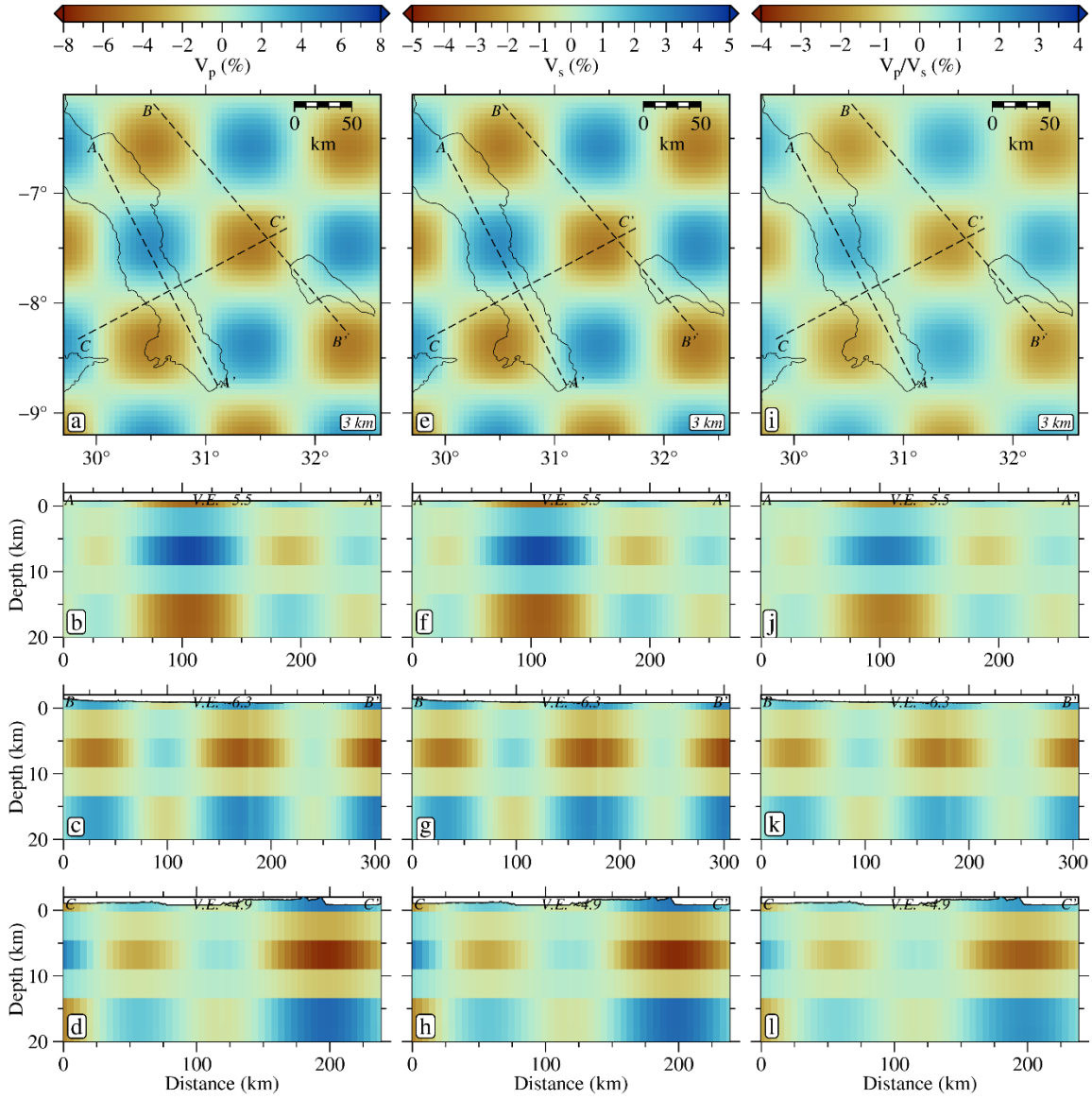

Figure S6. True synthetic model with 100 km x 100 km x 12.5 km checkers.

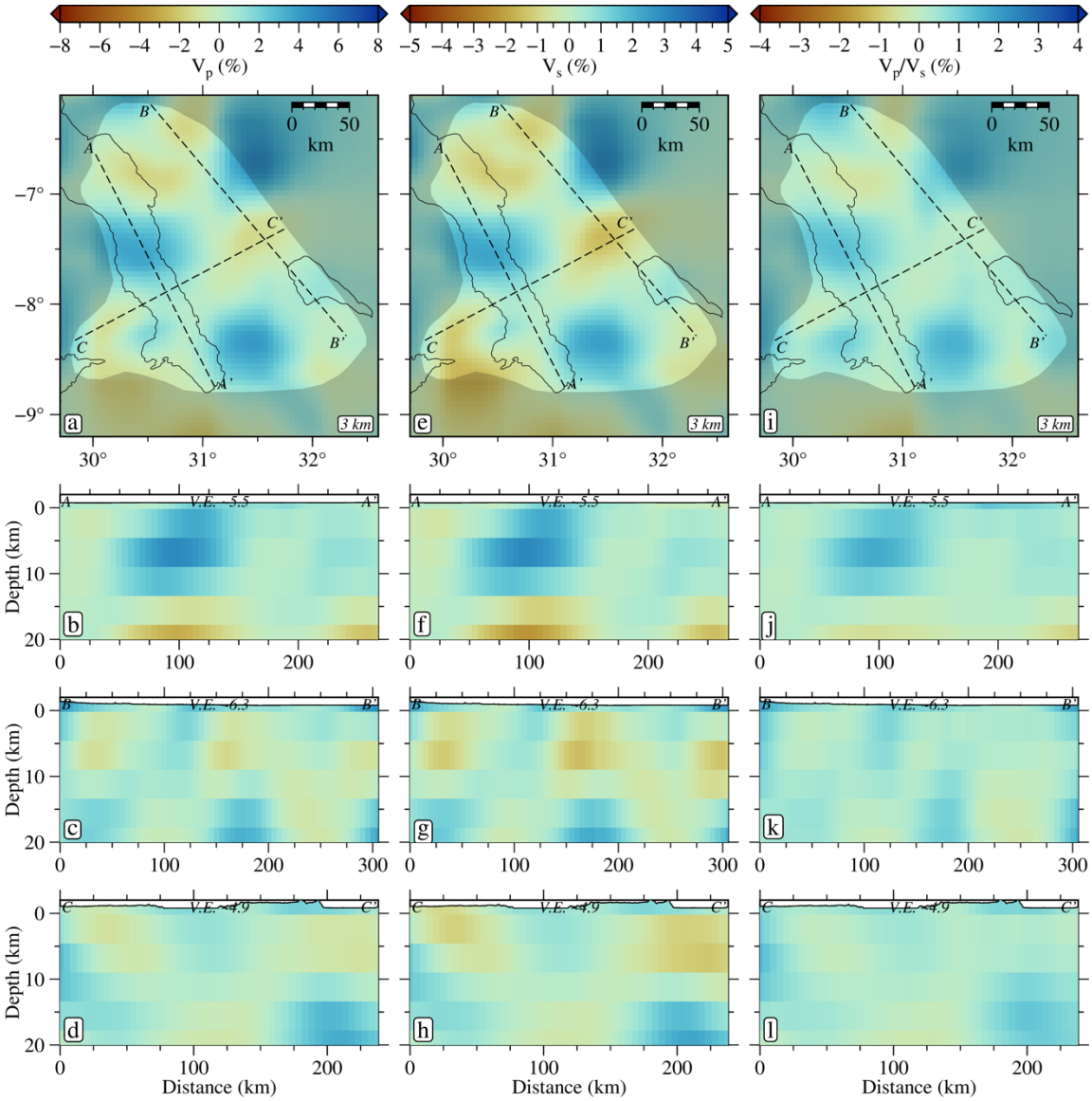

Figure S7. Recovered synthetic model with 100 km x 100 km x 12.5 km checkers. Unreliable areas of the models are lightly grayed out on the maps.

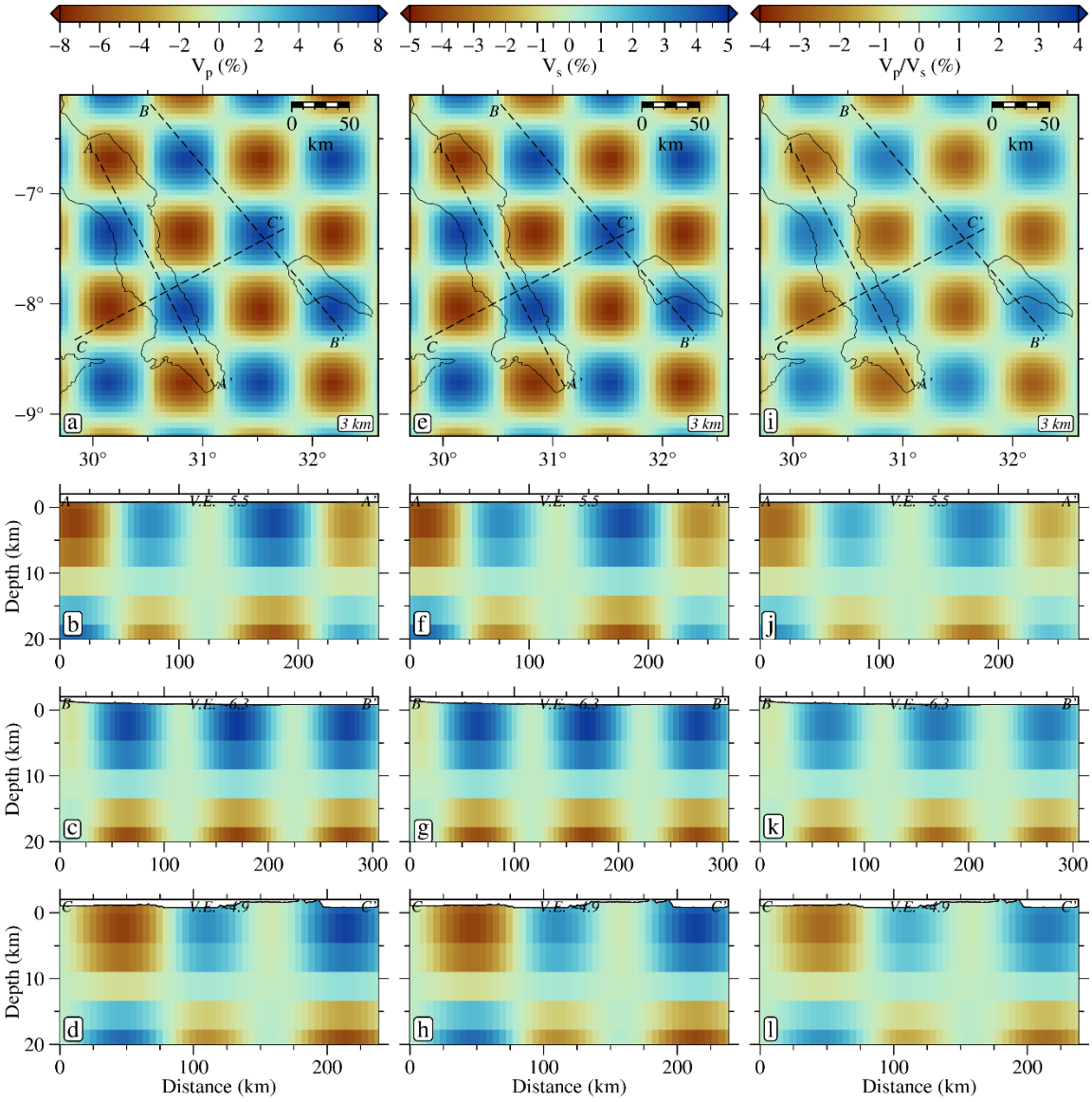

Figure S8. True synthetic model with 75 km x 75 km x 25 km checkers.

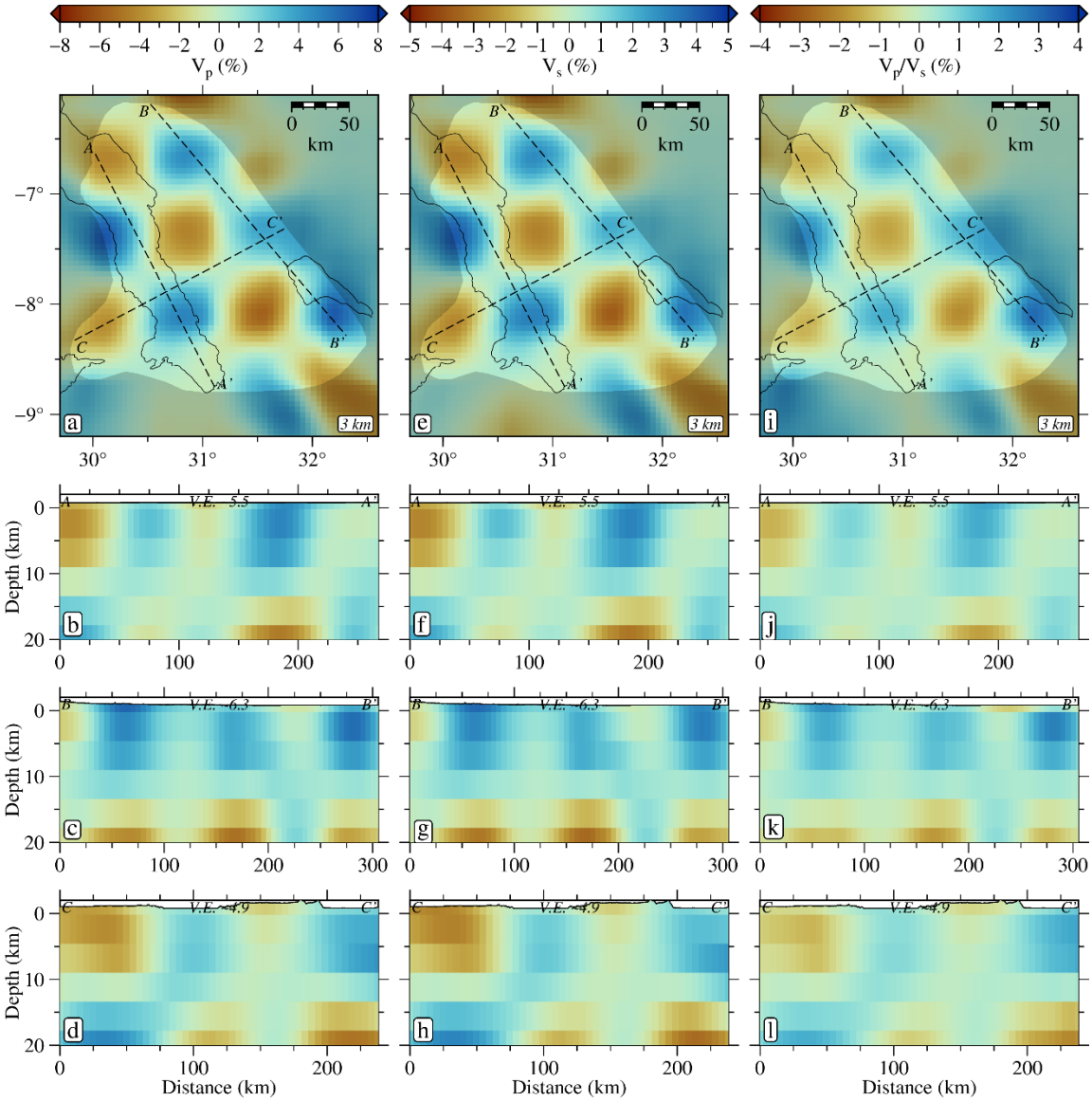

Figure S9. Recovered synthetic model with 75 km x 75 km x 25 km checkers. Unreliable areas of the models are lightly grayed out on the maps.

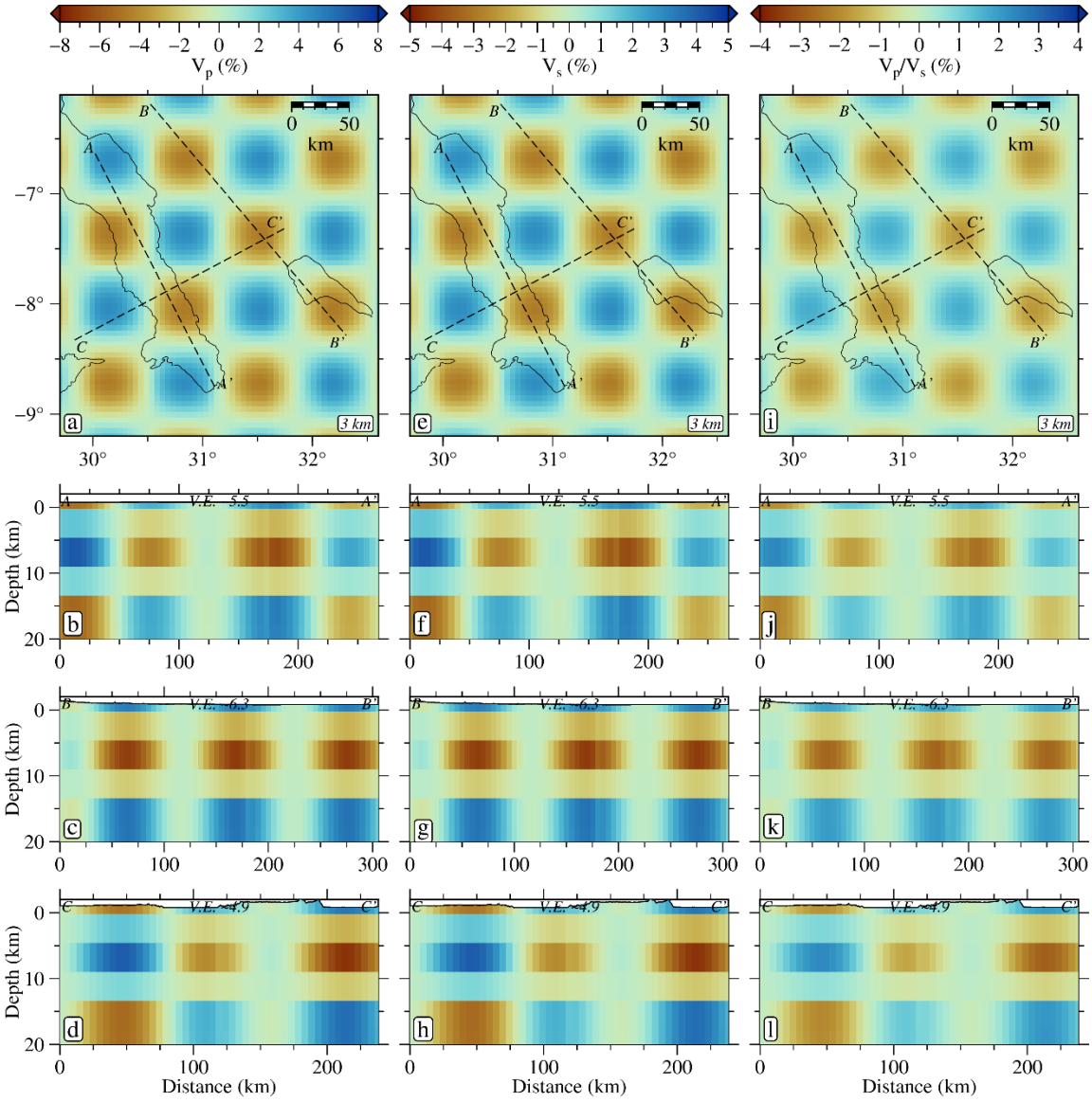

Figure S10. True synthetic model with 75 km x 75 km x 12.5 km checkers.

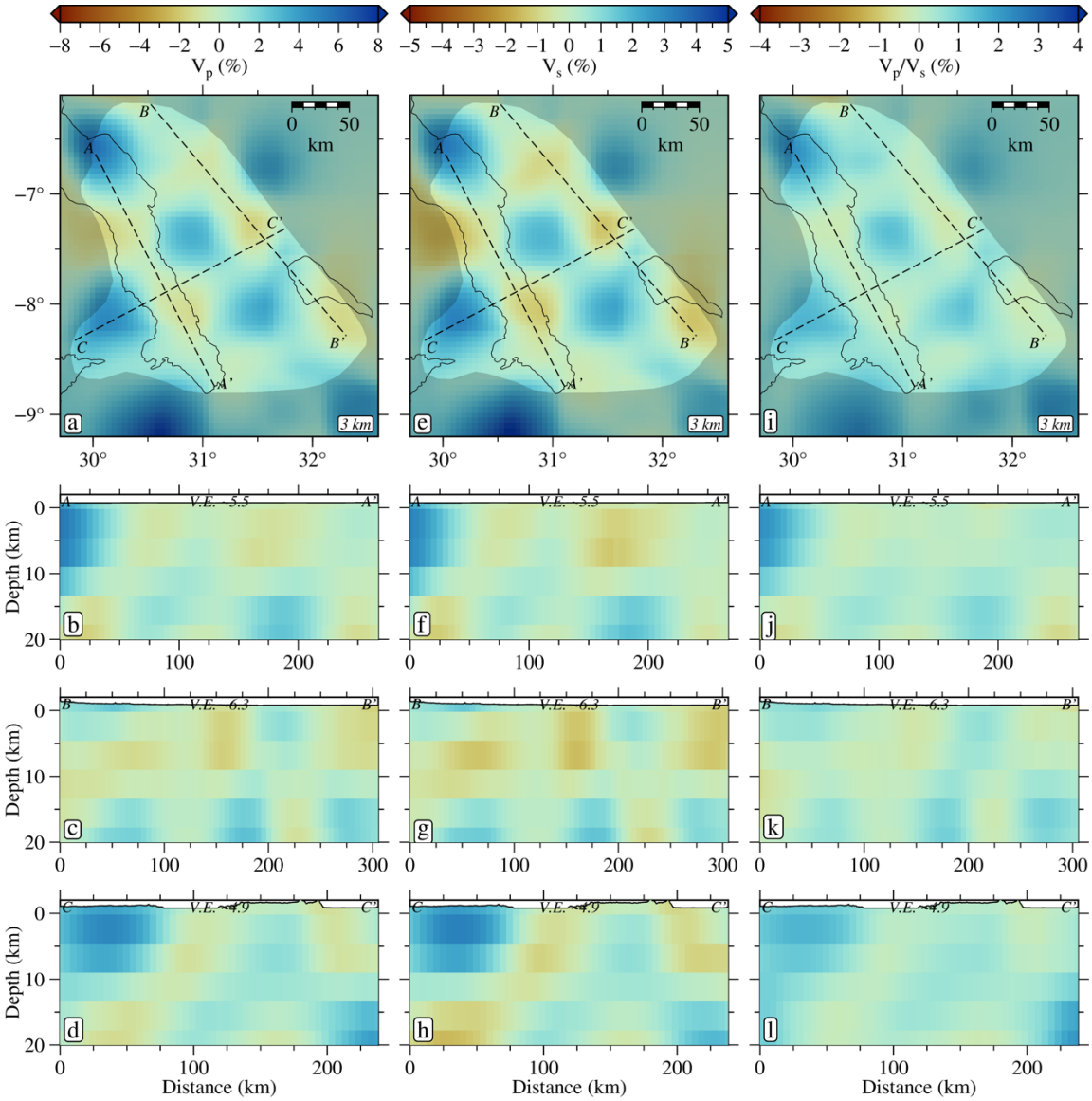

Figure S11. Recovered synthetic model with 75 km x 75 km x 12.5 km checkers. Unreliable areas of the models are lightly grayed out on the maps.

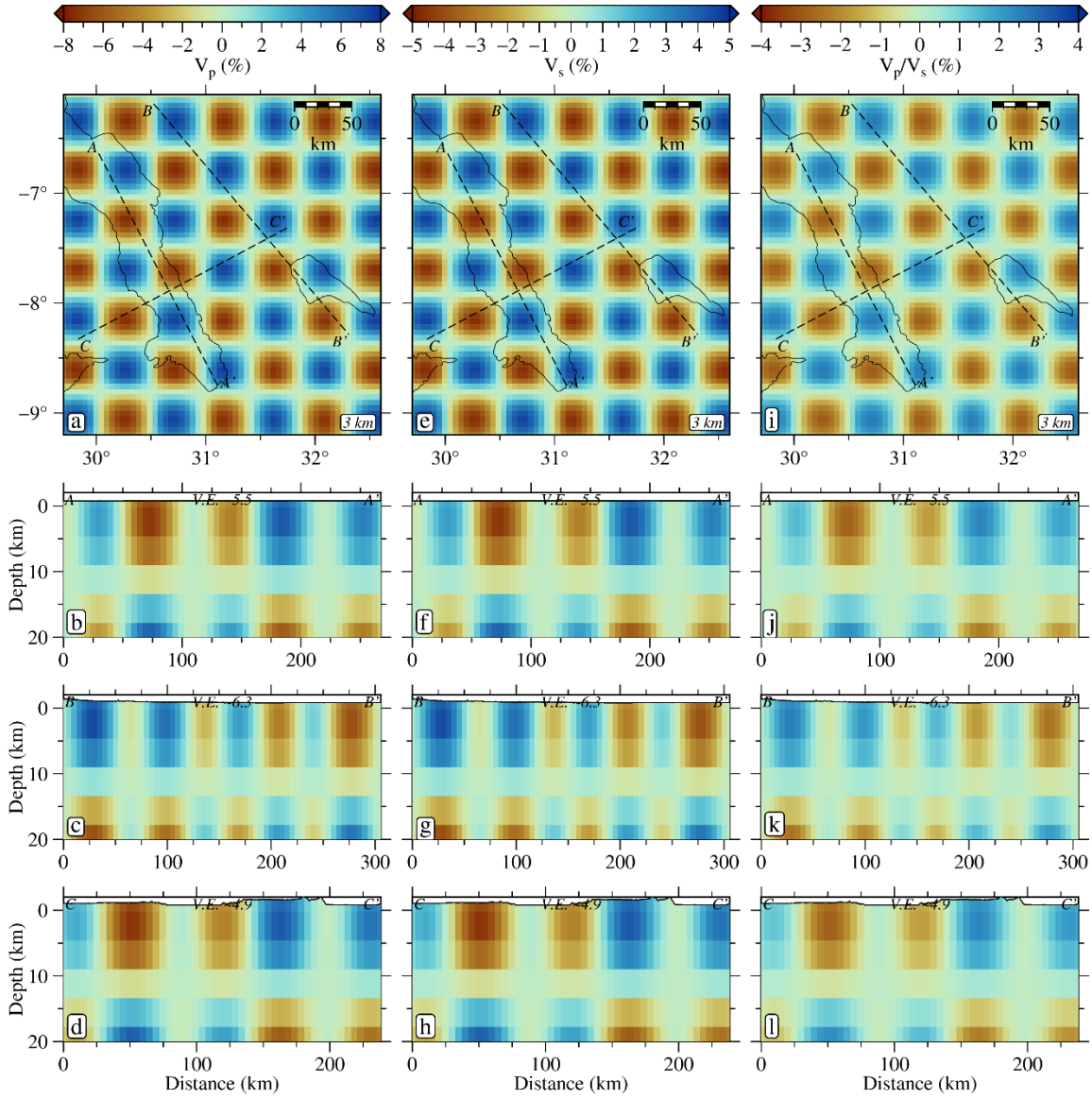

Figure S12. True synthetic model with 50 km x 50 km x 25 km checkers.

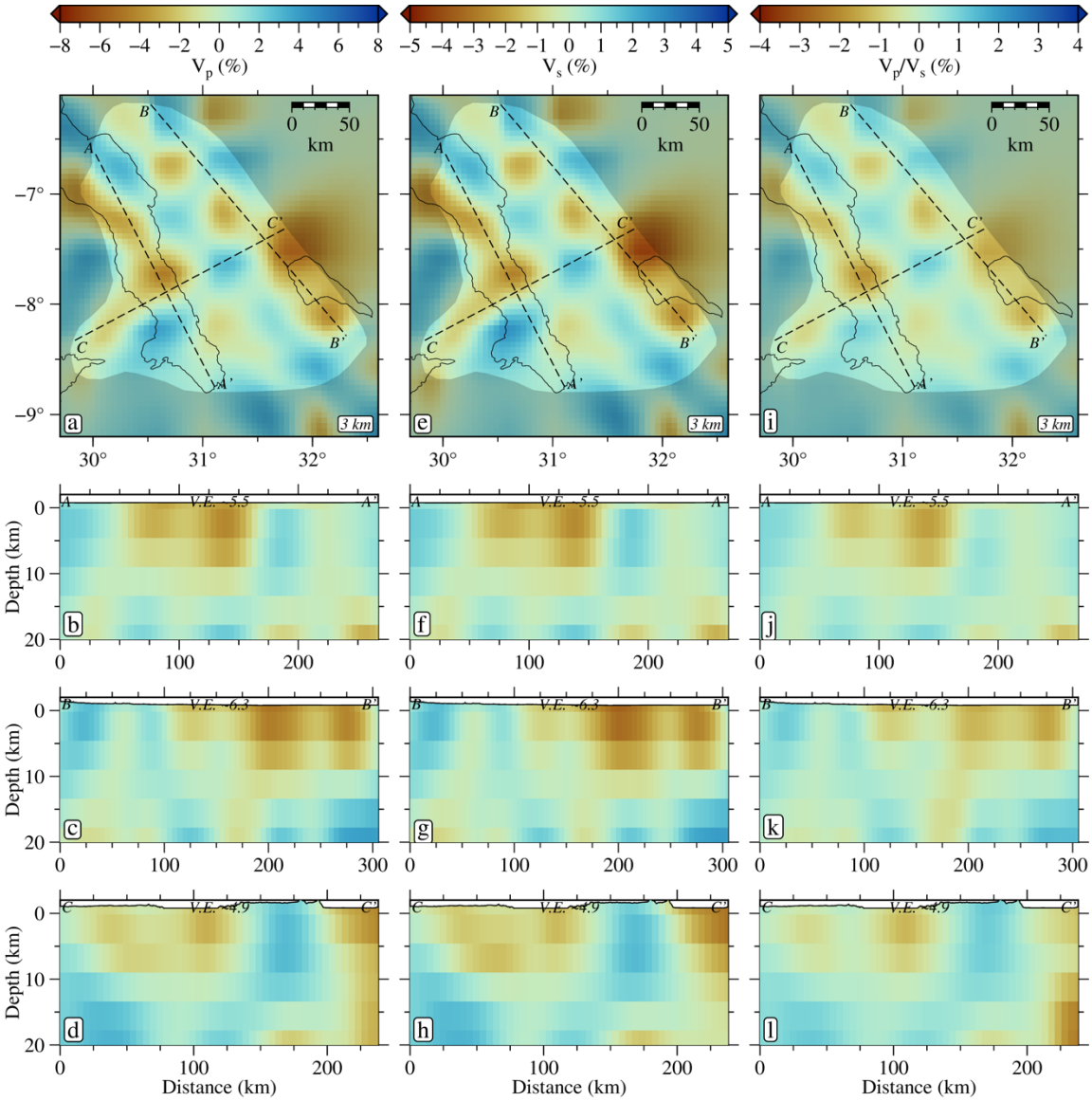

Figure S13. Recovered synthetic model with 50 km x 50 km x 25 km checkers. Unreliable areas of the models are lightly grayed out on the maps.

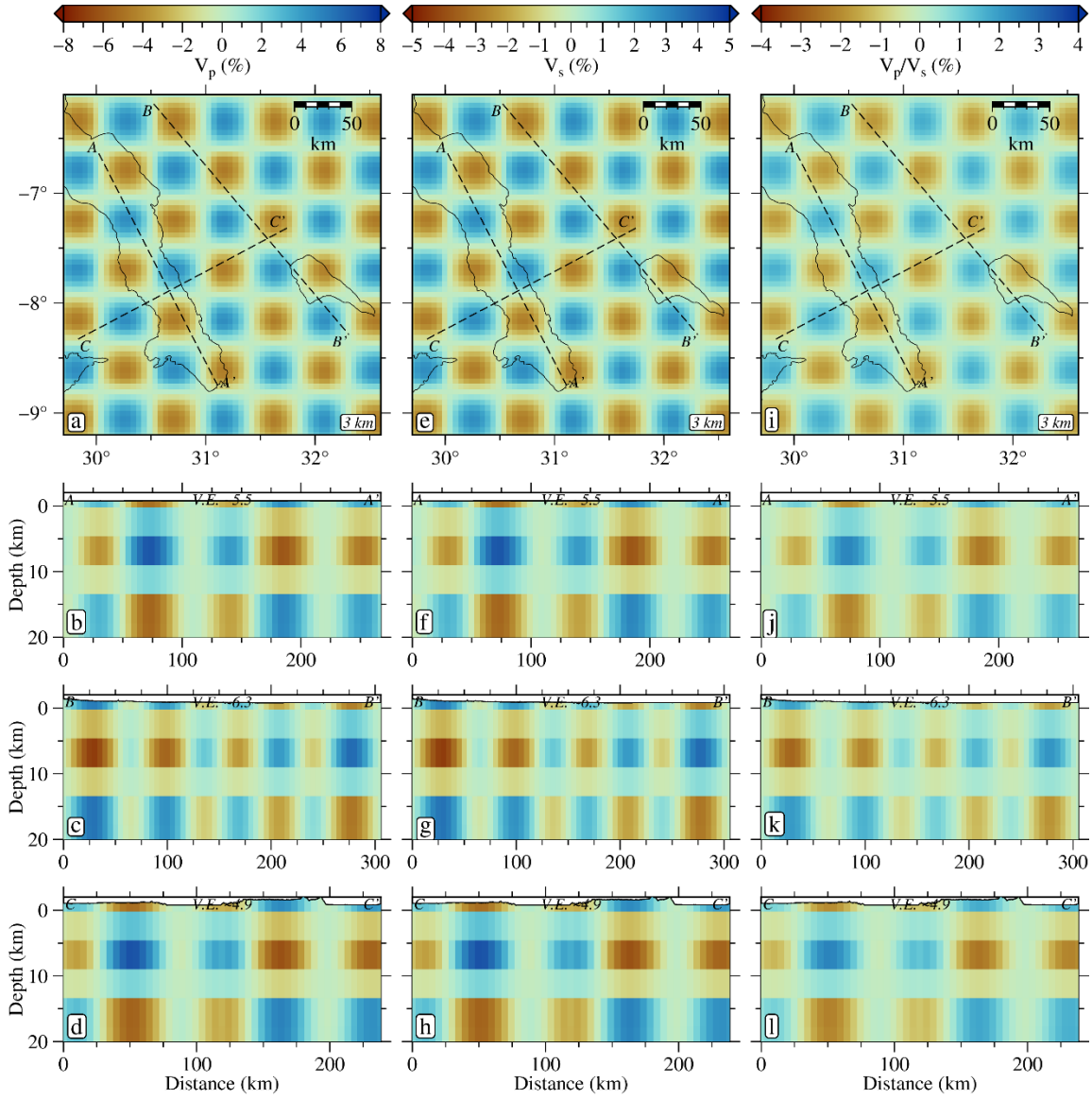

Figure S14. True synthetic model with 50 km x 50 km x 12.5 km checkers.

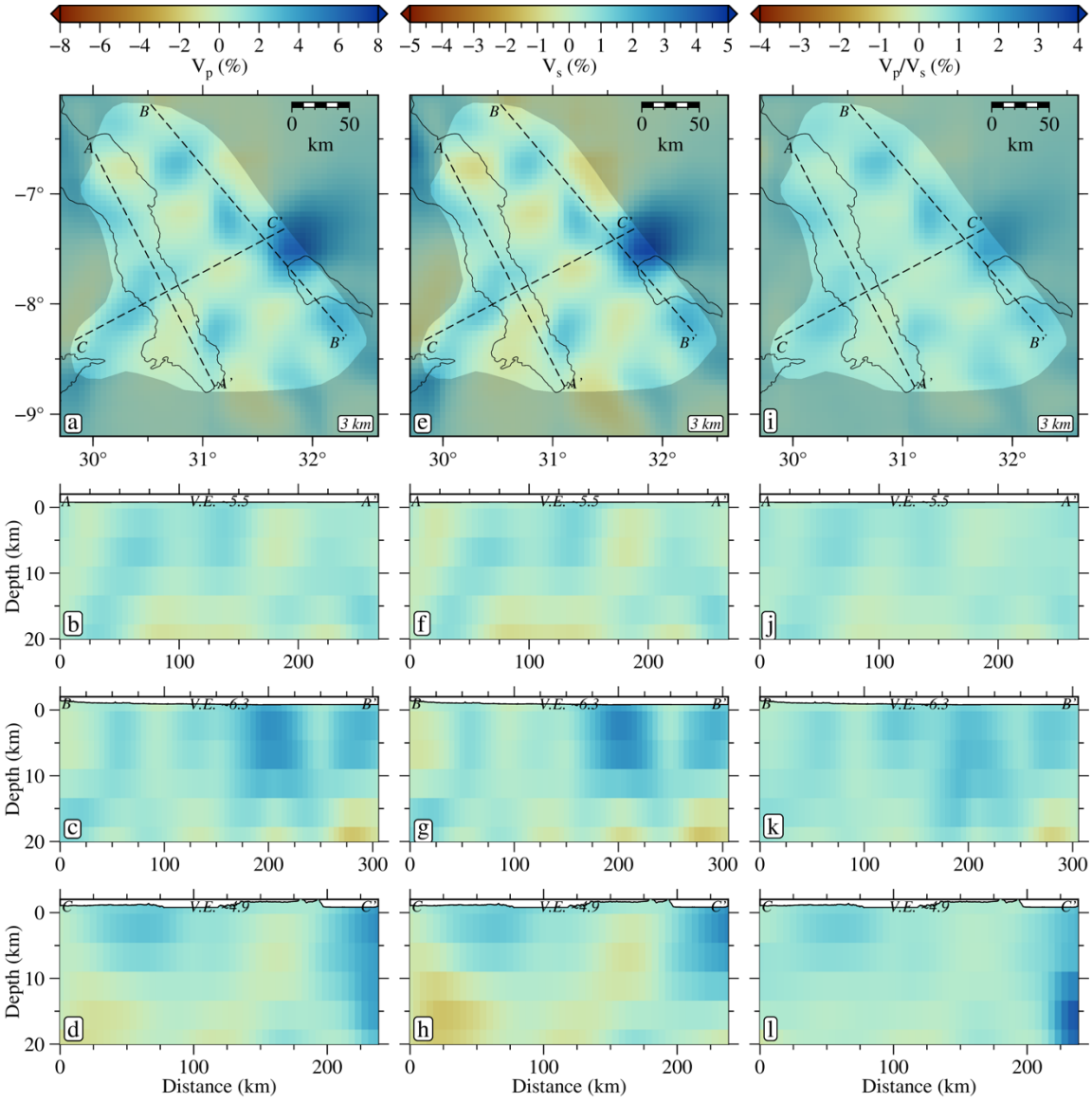

Figure S15. Recovered synthetic model with 50 km x 50 km x 12.5 km checkers. Unreliable areas of the models are lightly grayed out on the maps.

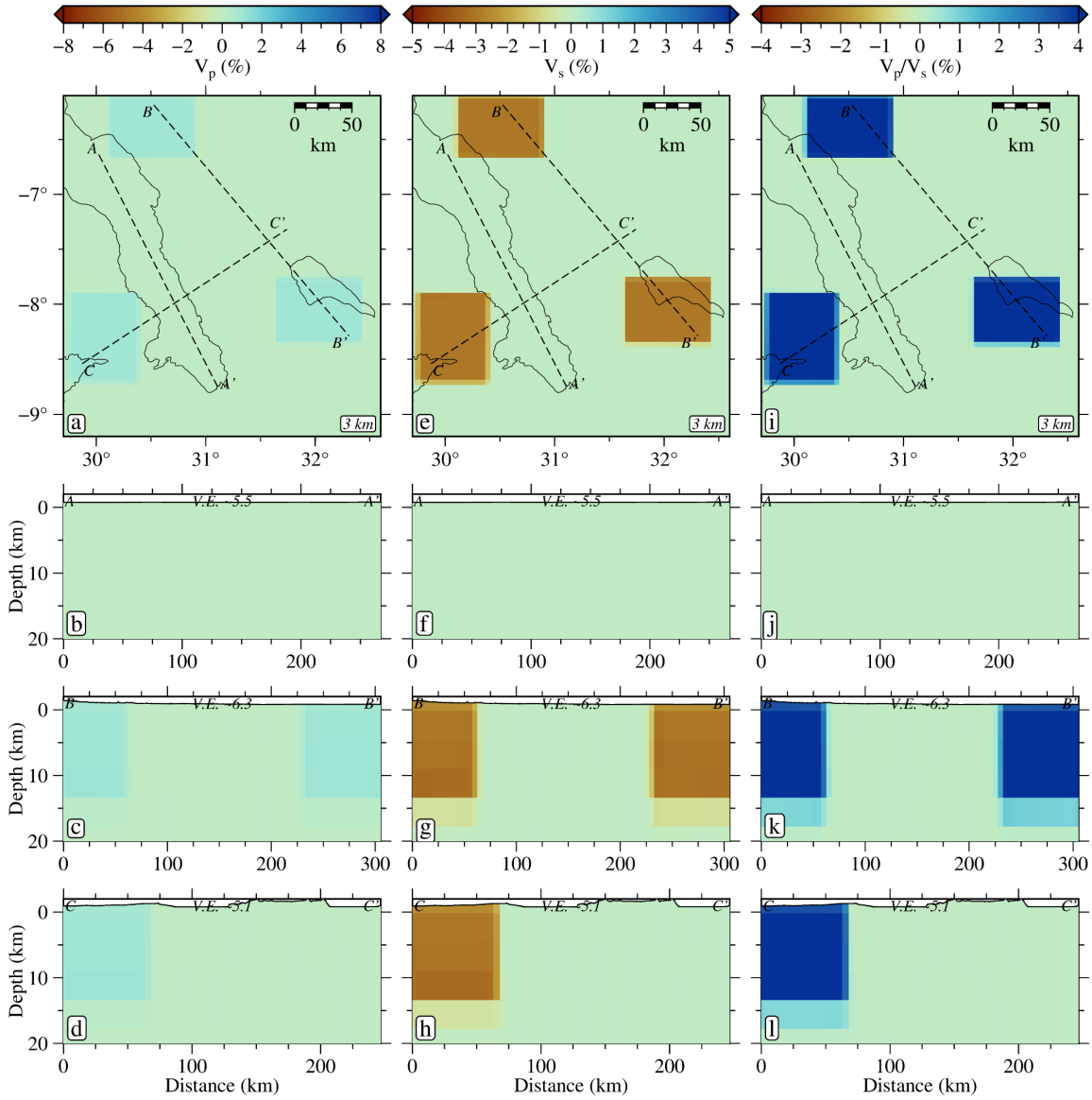

Figure S16. True custom synthetic model generated by perturbing the P (1% increase) and S (3% decrease) velocity models to generate three Vp/Vs (~4 % increase) anomalies. (**a**) 3 km depth slice through the P wave velocity model. Dashed black lines show the profile locations in b - l. (**b** – **d**) Profiles of the P wave velocity model. (**e** – **h**) Same as a-d but for the S wave velocity model. (**i** – **l**) Same as a-d but for the Vp/Vs ratios.

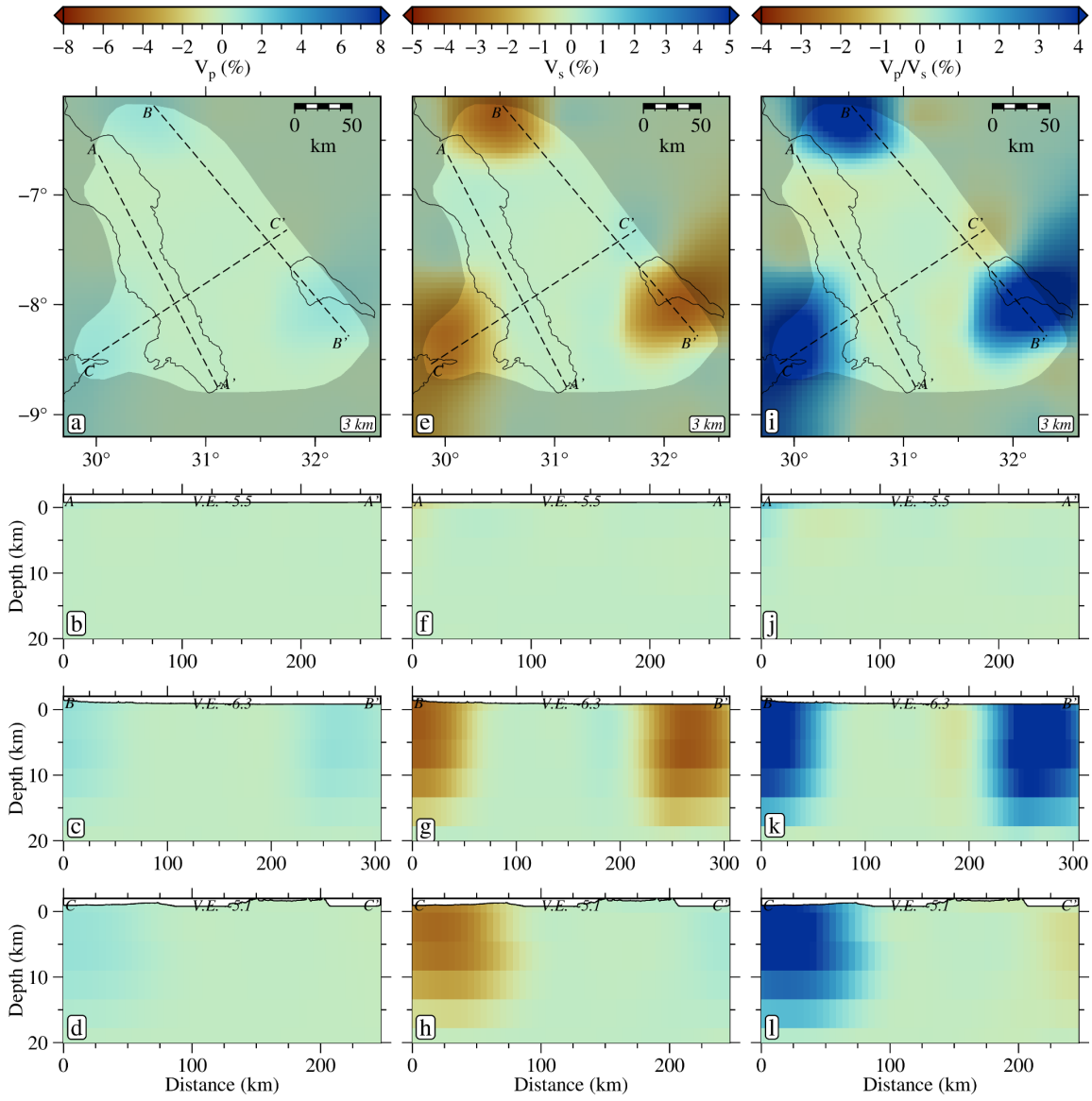

Figure S17. Recovered custom synthetic model from Fig. S16. (**a**) 3 km depth slice through the P wave velocity model. Dashed black lines show the profile locations in in b - l. Unreliable areas of the model are lightly grayed out. (**b** – **d**) Profiles of the P wave velocity model. (**e** – **h**) Same as a-d but for the S wave velocity model. (**i** – **l**) Same as a-d but for the Vp/Vs ratios.

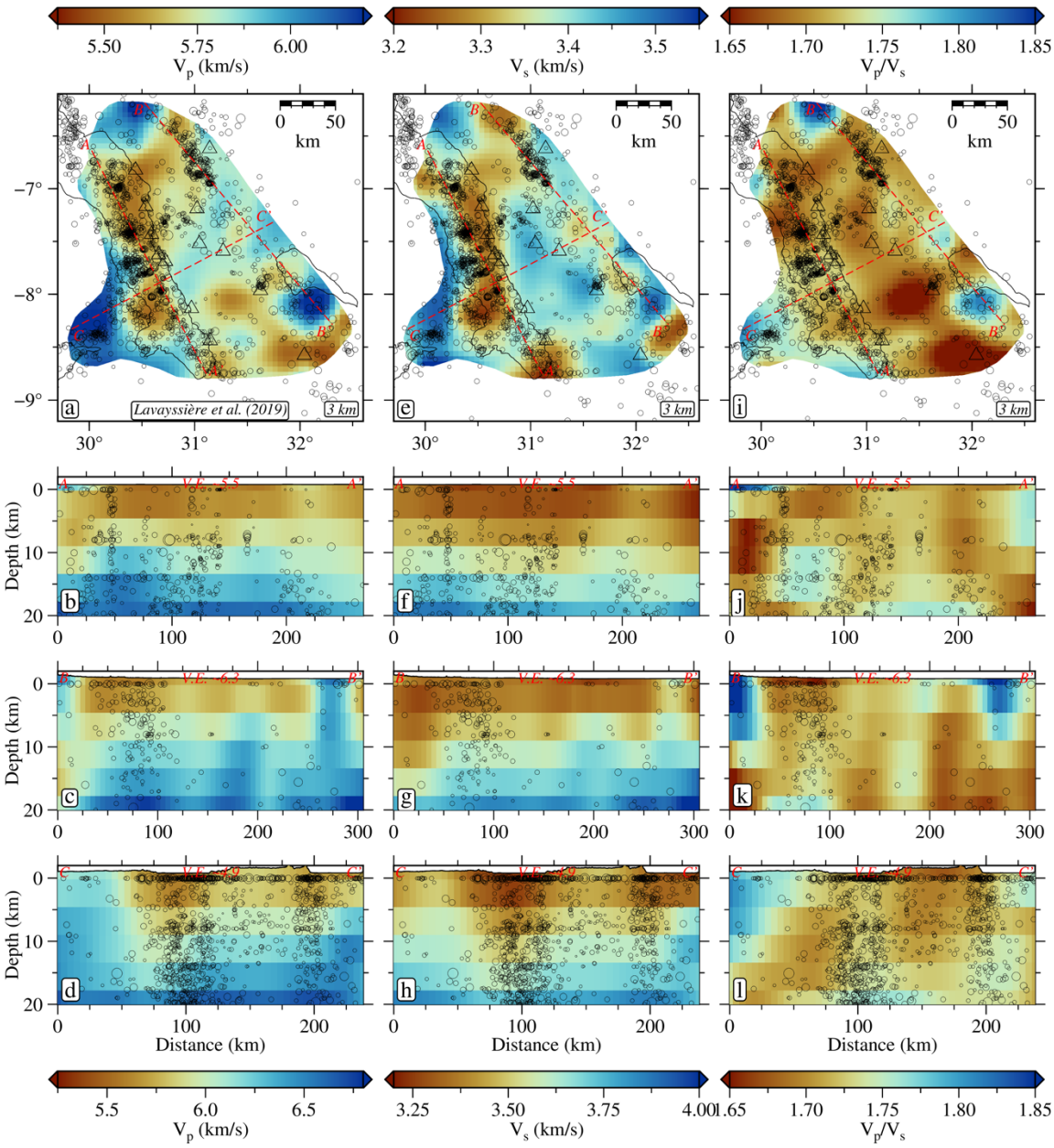

Figure S18. Same as Figure 3 in the manuscript but showing the absolute values of the model parameters rather than perturbations relative to the starting 1D models of Lavayssière et al. (2019).

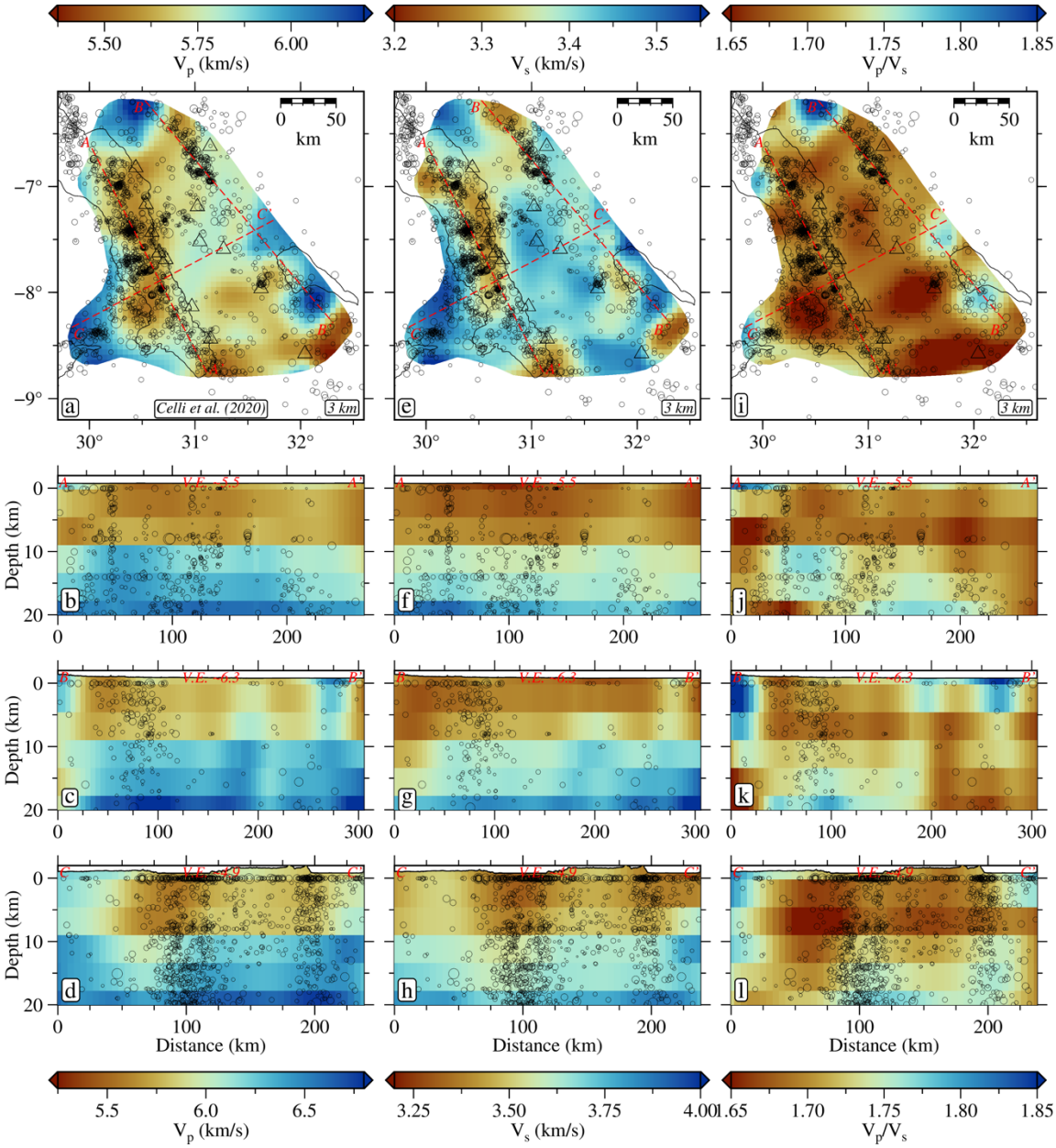

Figure S19. Inverted model results using the 3D regional P and S tomographic models of Celli et al. (2020) as starting models.

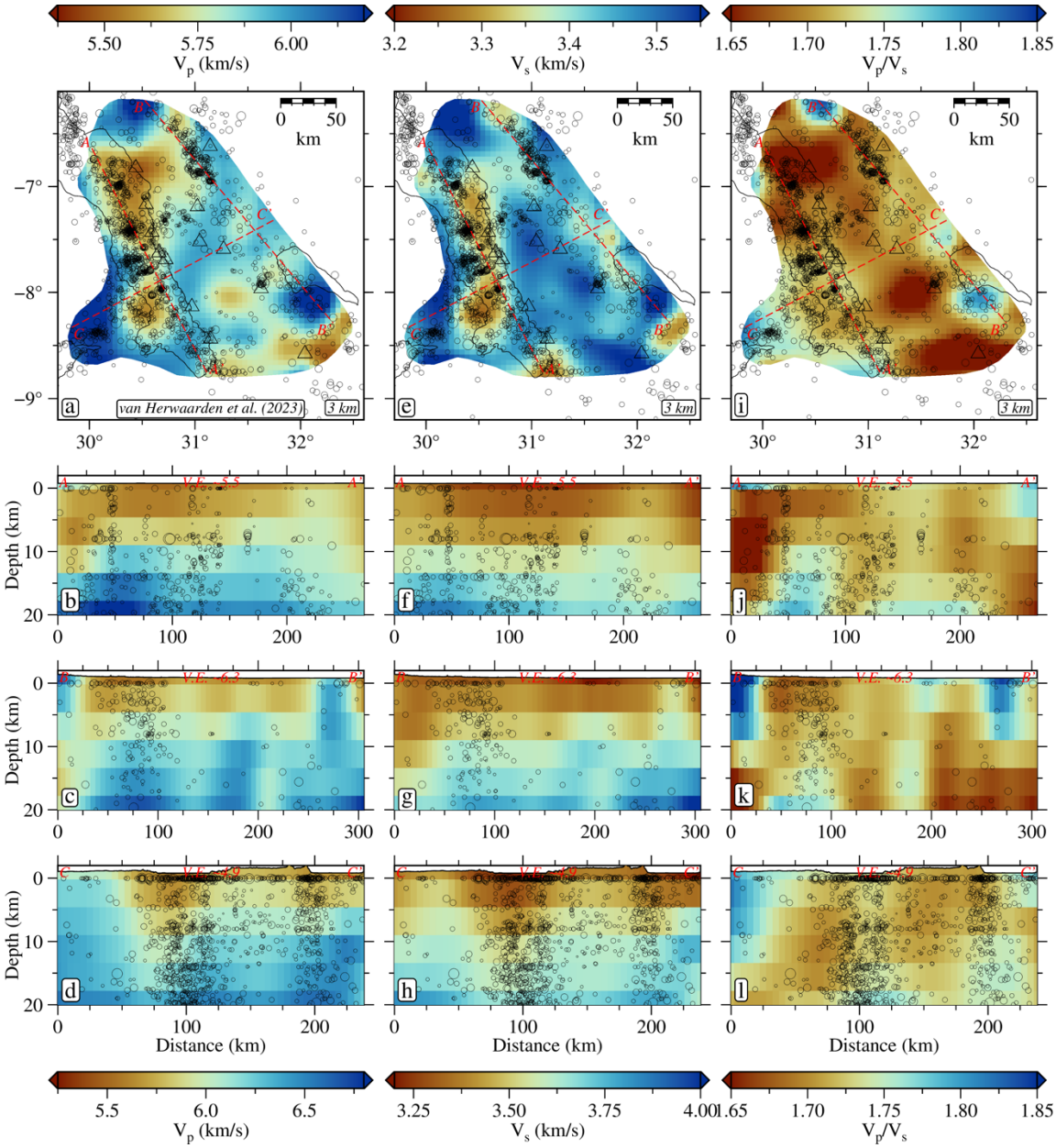

Figure S20. Inverted model results using the 3D regional P and S tomographic models of van Herwaarden et al. (2023) as starting models.

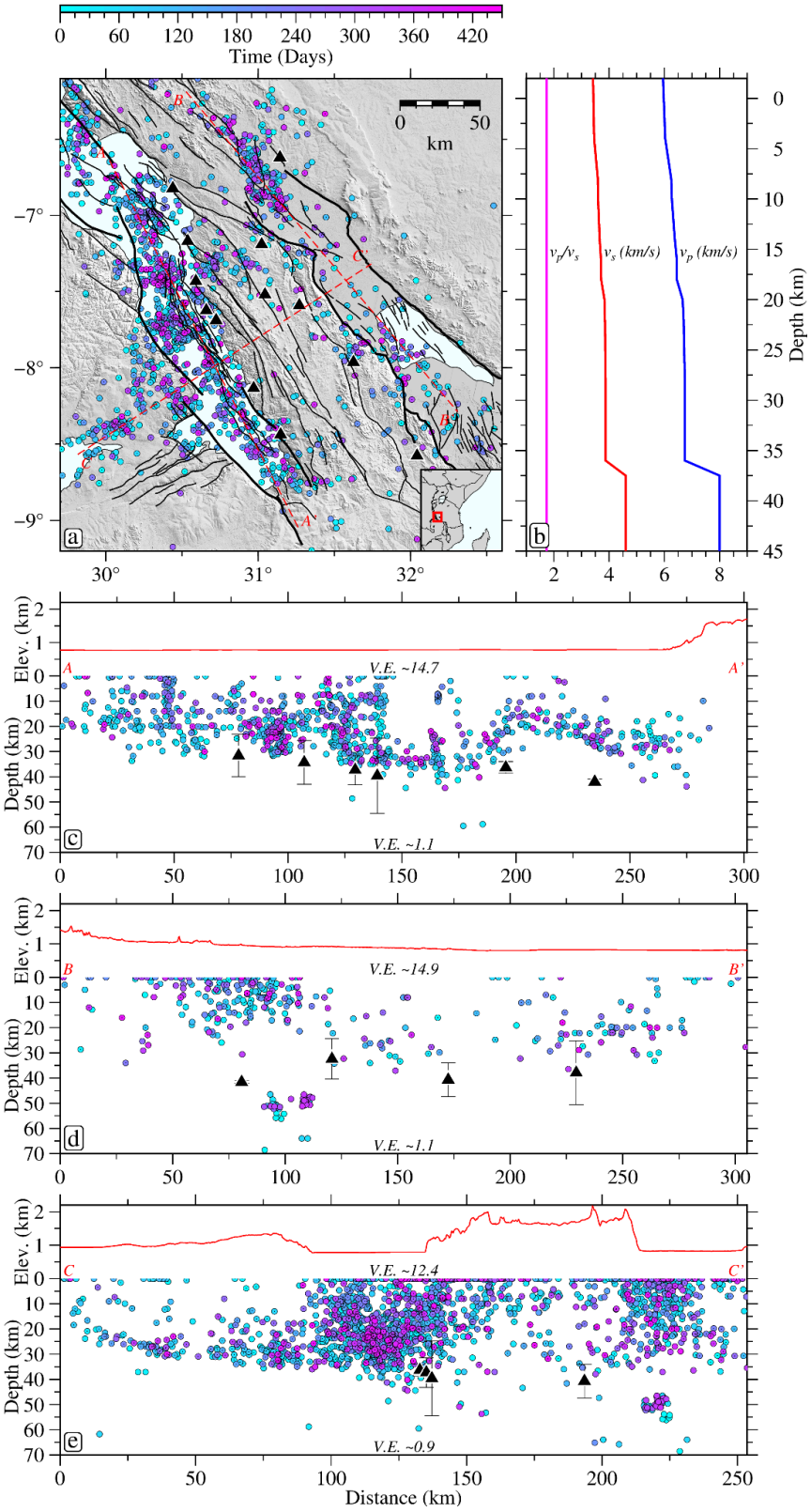

Figure S21. Similar to Fig. 2, with the seismicity colored according to their occurrence time relative to the earliest event in the catalog.

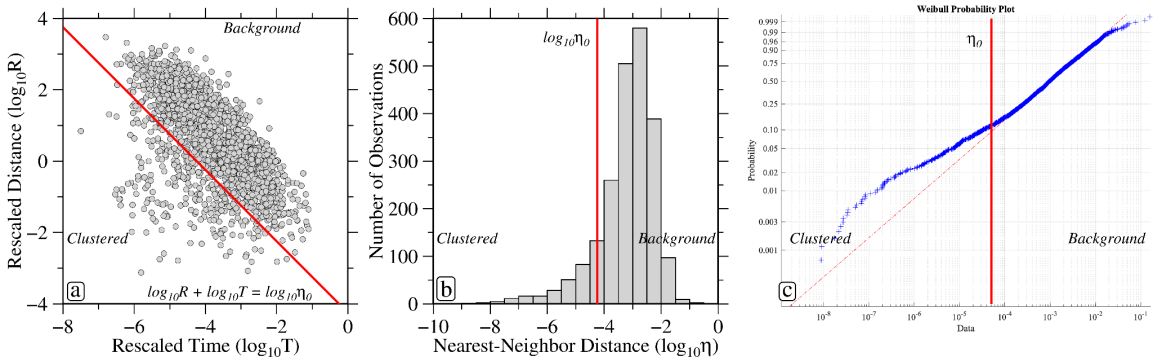

Figure S22. Cluster analysis result. (**a**) Map of time (T) and distance (R) components of the nearest-neighbor distance for each earthquake in the catalog. The red line separates the clustered events (below the line) from the background events (on or above the line). (**b**) Histogram showing the distribution of the nearest-neighbor distances. (**c**) Probability plot comparing the distribution of the nearest-neighbor distances (blue plus symbols) to a Weibull distribution (red dashed line). The deviation of the data from the Weibull distribution indicates that the seismicity does not represent a Poissonian (background) catalog. The deviation occurs approximately around the estimated separation threshold (red line).

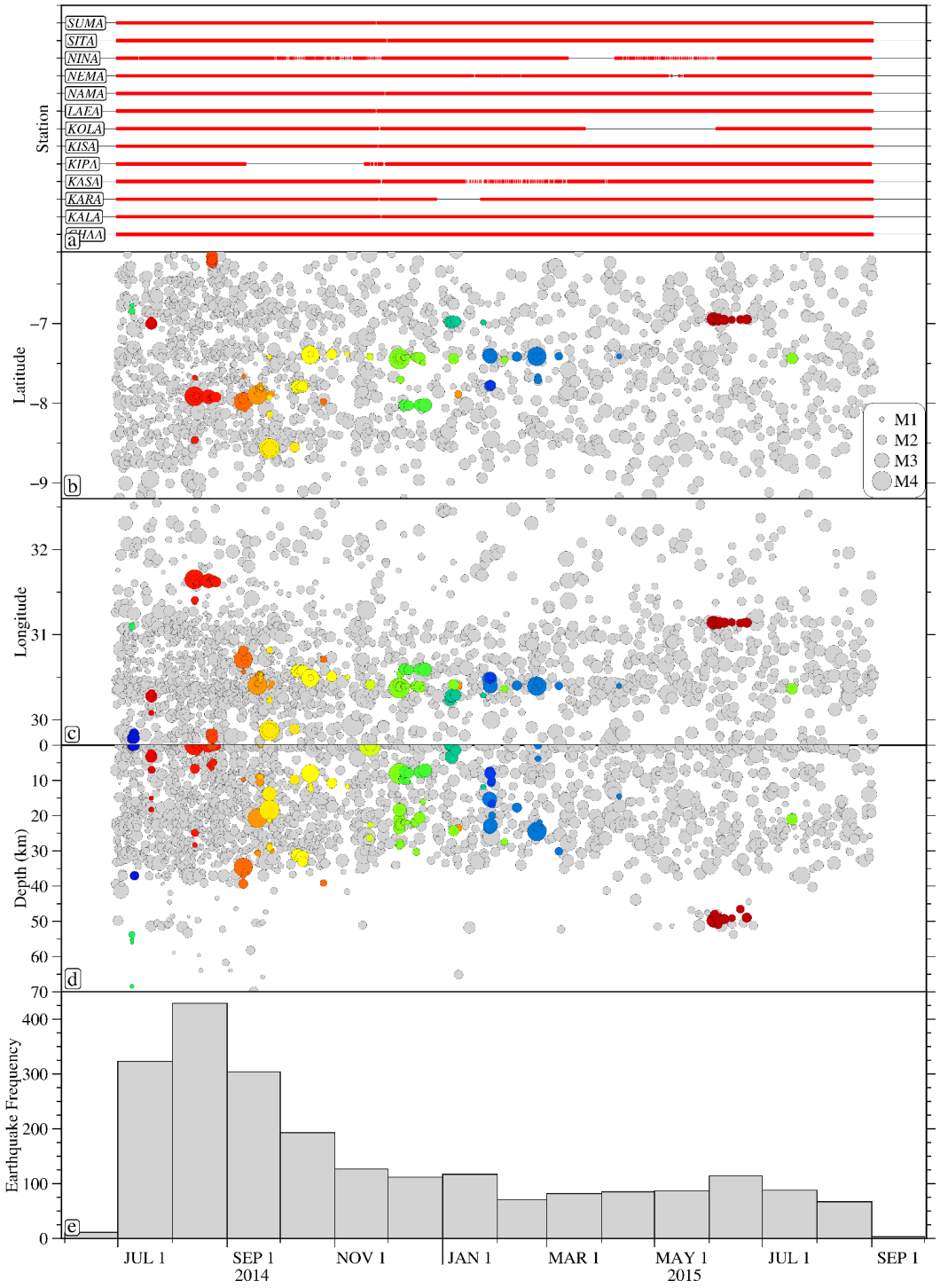

Figure S23. Network data continuity, earthquake clusters, and seismicity distribution as functions of time. (**a**) Data availability plot for stations in the TANGA14 array. The red line indicates periods when the seismometer was operational. (**b**) Seismicity as a function of time and latitude. Clusters are colored. (**c**) Same as panel b but as a function of longitude. (**d**) Same as panel b but as a function of depth. (**e**) Histogram of the events in the catalog for each month during deployment.

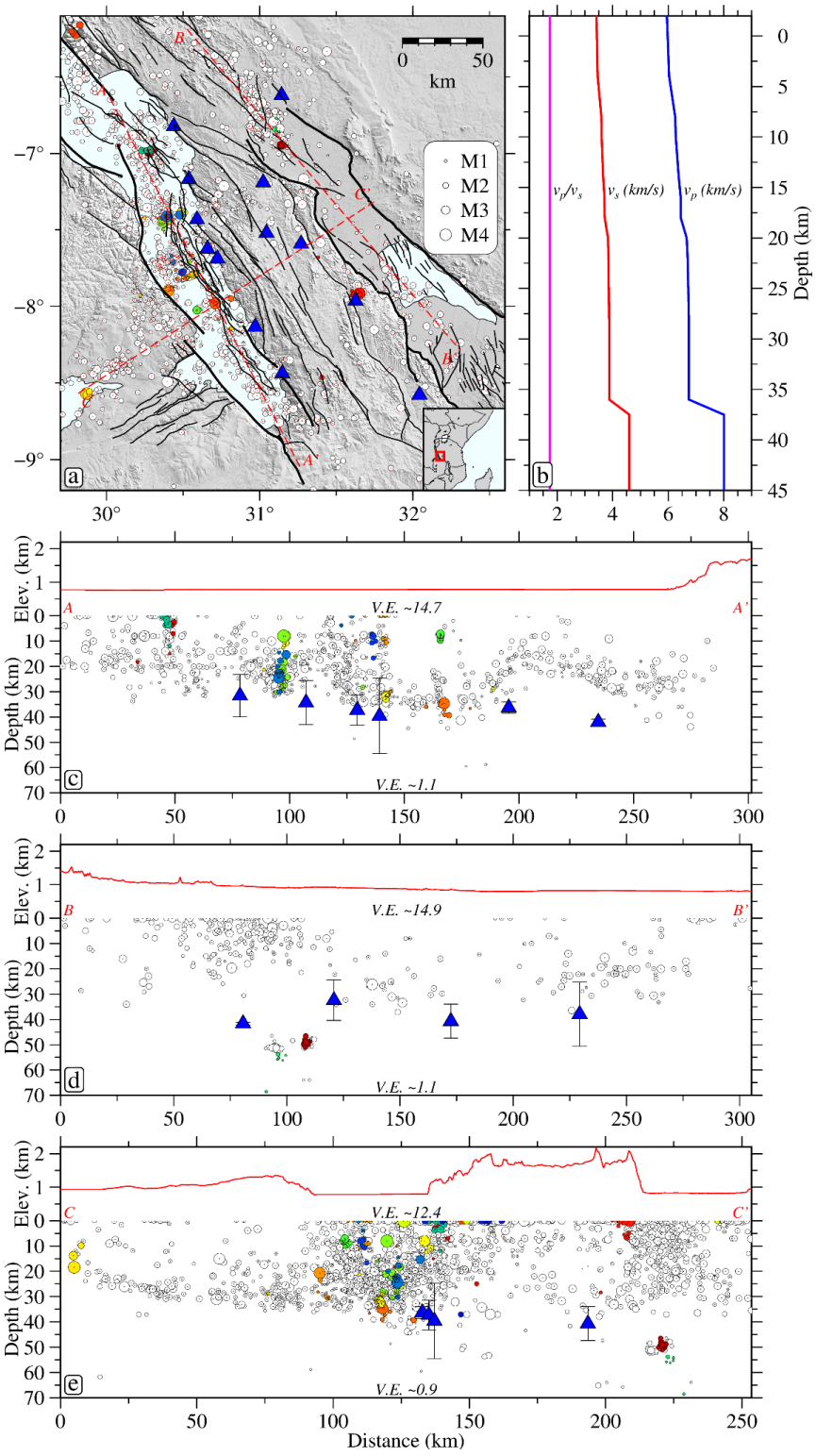

Figure S24. Similar to Fig. 2, with the clusters highlighted (colored circles).

References

Celli, N. L., Lebedev, S., Schaeffer, A. J., & Gaina, C. (2020). African cratonic lithosphere carved by mantle plumes. *Nature Communications, 11*(92), 1-10.

Lavayssière, A., Drooff, C., Ebinger, C. J., Gallacher, R., Illsley-Kemp, F., Oliva, S. J., & Keir, D. (2019). Depth Extent and Kinematics of Faulting in the Southern Tanganyika Rift, Africa. *Tectonics, 38*, 842-862.

van Herwaarden, D., Thrastarson, S., Halpa, V., Afanasiev, M., Trampert, J., & Fichtner, A. (2023). Full-Waveform Tomography of the African Plate Using Dynamic Mini-Batches. *Journal of Geophysical Research: Solid Earth, 126*, 1-22.